

Article

# Structural Parametric Optimization of the VoltornUS-S Semi-Submersible Foundation for a 15 MW Floating Offshore Wind Turbine

Shiqi Liu <sup>1</sup>, Zhenju Chuang <sup>1,\*</sup>, Kai Wang <sup>2</sup>, Xin Li <sup>3</sup>, Xin Chang <sup>1,\*</sup> and Lixun Hou <sup>1</sup>

<sup>1</sup> Naval Architecture and Ocean Engineering College, Dalian Maritime University, Dalian 116026, China

<sup>2</sup> School of Ocean Engineering and Technology, Sun Yat-sen University, Zhuhai 510275, China

<sup>3</sup> State Key Laboratory of Coastal and Offshore Engineering, Dalian University of Technology, Dalian 116024, China

\* Correspondence: zhenjuchuang@dlnu.edu.cn (Z.C.); xin.chang@dlnu.edu.cn (X.C.)

**Abstract:** The full exploitation of offshore wind resources can essentially satisfy the massive energy demand. The realization and application of ultra-high-power offshore wind turbines are crucial to achieving full use of deep-sea wind energy and reducing the cost of wind power. For the VoltornUS-S semi-submersible floating foundation of a 15 megawatt (MW) offshore wind turbine, the effect of structural parameters on hydrodynamic performance was investigated by controlling the variables described in this paper. Accordingly, the floating foundation was optimized and coupled to the 15 MW offshore wind turbine. The dynamic performance of the integrated 15 MW offshore wind turbine was analyzed under different operating conditions, by applying the aero-hydro-servo-elastic coupled method. The results show that for a wave in a 0-degree direction, a 5% increase of column spacing will reduce the peak value of the pitch transfer function by 33.61%, and that a 5% decrease of the outer column diameter will further reduce the peak value by 26.27%. The standard deviation of the time-domain surge responses was reduced by 19.78% for the optimized offshore wind turbine, and the maximum value of the mooring line tension was reduced by 13.55% under normal operating conditions.

**Keywords:** floating offshore wind turbine; 15 MW offshore wind turbine; structural parametric optimization; floating foundation; dynamic response; hydrodynamic performance



**Citation:** Liu, S.; Chuang, Z.; Wang, K.; Li, X.; Chang, X.; Hou, L. Structural Parametric Optimization of the VoltornUS-S Semi-Submersible Foundation for a 15 MW Floating Offshore Wind Turbine. *J. Mar. Sci. Eng.* **2022**, *10*, 1181. <https://doi.org/10.3390/jmse10091181>

Academic Editor: José Correia

Received: 9 July 2022

Accepted: 18 August 2022

Published: 24 August 2022

**Publisher's Note:** MDPI stays neutral with regard to jurisdictional claims in published maps and institutional affiliations.



**Copyright:** © 2022 by the authors. Licensee MDPI, Basel, Switzerland. This article is an open access article distributed under the terms and conditions of the Creative Commons Attribution (CC BY) license (<https://creativecommons.org/licenses/by/4.0/>).

## 1. Introduction

Offshore wind energy has recently been paid wider attention. The Floating Offshore Wind Turbine (FOWT), equipment for exploiting offshore wind energy, has developed rapidly. By 2050, the energy that offshore wind can provide will be equivalent to that of offshore oil resources, the production of which will shrink by 51% compared to 2019 [1]. In 2021, new installations of offshore wind turbines accounted for 22.5% of the total new installations of wind turbines. The global installed capacity of offshore wind turbines was 57 gigawatt (GW), accounting for 7% of worldwide total installed capacity in 2021 [2]. With the continuous utilization of offshore wind energy, offshore wind farms are gradually developing from shallow waters to deep waters in order to fully exploit abundant offshore wind resources [3]. Floating offshore wind energy is likely to expand rapidly to meet the world's capacity needs [2]. Due to the high cost of construction, transportation, installation, and maintenance of the offshore wind turbines, offshore wind turbines are gradually showing a trend towards higher power and larger scale to reduce the cost of wind power.

Chuang et al. [4] studied the impact of second-order hydrodynamic loads on the dynamic performance of the National Renewable Energy Laboratory (NREL)'s 5 MW FOWT. Their results showed that when affected by the second-order slow-drift wave force, the

motion of the offshore wind turbine increased significantly in the wave propagation direction, with a consequent increase in the mooring line's tension. Zhao et al. [5] investigated the effect of second-order wave loads on a 10 MW and 5MW floating semi-submersible wind turbines, from aspects of the structure and hydrodynamic performance. The results showed that the low-frequency motions of the wind turbine became more significant and the mooring line tension was noticeably changed when the difference-frequency wave loads were considered. The sum-frequency wave loads markedly affected the structural responses. In addition, the effect of second-order wave loads on the 10 MW floating wind turbine was more prominent than on the 5 MW turbine. Liu et al. [6] made a coupling analysis of a 15 MW floating wind turbine in multiple severe environmental conditions and considered the effect of difference-frequency wave loads. The results showed that compared with a moderate sea state, the impact of difference-frequency wave forces on the motion responses and mooring line tension was more significant in a typhoon sea state.

Investigating the floating foundations of offshore wind turbines, Zhou et al. [7] performed a sensitivity analysis on the dimension parameters of four-column and Y-shaped semi-submersible foundations. Based on the results of the sensitivity analysis, the dimension parameter optimization of the two semi-submersible foundations was calculated with the aid of the genetic algorithm. The results of the sensitivity analysis showed that the draft depth, column radius, and column spacing affected the first-order hydrodynamic response of the floating foundation. Ren et al. [8] studied the dynamic performance of a Tension Leg Platform (TLP) FOWT in the event of tendon rupture. The results show that failure of the tendon affected the heave, pitch, and roll responses of the FOWT. In addition, the intact tendon adjacent to the ruptured tendon was subjected to double the average tensile force. Yi et al. [9] investigated the configuration parameters of different floating foundations of 5 MW offshore wind turbines and analyzed their dynamic responses. The results showed that for the OC4-DeepCwind semi-submersible foundation, the column diameter and thickness of the base column affected the wave loads on the floating foundation. Wei et al. [10] designed a new type of semi-submersible foundation for a 5 MW wind turbine, composed of a large circular ballast tank at the bottom and three outer columns connected to the central column by the pontoons at the water plane. The stability and hydrodynamic performance of this new floating foundation were analyzed, and the time-domain responses of the 5 MW offshore with this new foundation were investigated under various environmental conditions. The investigation showed that the 5 MW offshore wind turbine with this new foundation demonstrated good stability and heave motion performance. Li et al. [11] designed a floating foundation for a 5 MW offshore wind turbine in shallow water. The foundation consists of an upper buoyancy column, an active ballast column, and a concrete ballast column below, connected centrally by truss members and arranged with two heave plates. Wang et al. [12] proposed a combined system consisting of a semi-submersible offshore wind turbine and a torus-type wave energy converter (WEC). They investigated the effect of different WEC shapes on the motion response and power performance of the combined energy system, and the hydrodynamic performance of the combined wind-wave energy converters was studied. The results showed that the combined energy converter with a concave WEC offered a superior dynamic response and larger power production. Cao et al. [13] carried out hydrodynamic analysis for a 10 MW offshore wind turbine using their newly designed floating foundation. They investigated the effects of different calculation methods for second-order wave forces on the dynamic responses of the wind turbine. The results showed that the pitch resonance responses calculated by the Newman approximation method and full QTF method were significantly different from the surge resonant response. The Newman approximation method was less accurate for calculating second-order wave loads.

There have been many studies on the performance optimization of the floating foundations for FOWTs. Wei and Zhao [14] utilized a bidirectional tuned liquid column damper (BTLCD) combined with a tuned mass damper (TMD), referred to as a bidirectional tuned liquid column mass damper (BTLCMD), to reduce the motion responses of a FOWT. The

results showed that the BTLCMD can effectively decrease the pitch, roll motion, and tower base loads of the floating wind turbine. Aboutalebi et al. [15] proposed a square-shaped platform barge with four oscillating water columns (OWCs) and applied a switching control strategy to reduce the oscillations of the FOWT. The results showed that the dynamic performance of the barge foundation could be optimized by controlling the OWCs' valves for different wave periods. Specifically, based on response amplitude operators (RAOs) analysis, the barge foundation with the OWC valves open had better dynamic performance in the case of the shorter wave periods (<12.35 s), and the performance of the standard barge and the closed-OWCs-based barge foundations were better when the wave period was larger than 12.35 s. Haji et al. [16] proposed a symbiotic energy-harvesting system combining the FOWT with an OC3 spar platform and a wave energy converter (WEC). The results showed that the motion resistance of the FOWT increased with a larger radius of WECs at larger wave frequencies, leading to reduction of the lateral responses. Accordingly, larger WECs can decrease the tower's lifetime fatigue stress; the WECs decreased the tower fatigue stress of the FOWT when their radii were larger than 8 m.

The above studies tended to focus on optimization of the foundation for a small-scale (5 MW) offshore wind turbine. Offshore wind turbines have shown a development trend towards a larger scale, but few researchers to date have aimed at improving the floating foundations which currently support large-scale offshore wind turbines. Allen et al. [17] described a UMaine VoltturnUS-S reference semi-submersible foundation to support the superstructure of a large-scale (15 MW) offshore wind turbine. The VoltturnUS-S floating foundation consists of four columns, with bottom pontoons and top cross braces. Niranjana et al. [18] investigated the dynamic responses of a 15 MW offshore wind turbine using the UMaine VoltturnUS-S semi-submersible foundation under different working conditions. Wu et al. [19] presented a method for upscaling a 5 MW wind turbine with the OC4 DeepCwind floating foundation to a 15 MW wind turbine. They compared it against a 15 MW wind turbine with the VoltturnUS-S floating foundation.

The optimization of the VoltturnUS-S floating foundation has not yet been realized. In order to achieve superior performance of the 15 MW FOWT, this paper focusses on the structural parameters of the UMaine VoltturnUS-S reference foundation. The outer column diameter and the distance from the outer columns to the central column were considered, and their effects on the hydrodynamic performance of the floating foundation were analyzed. Subsequently, the structural parameters of the semi-submersible foundation were optimized. Furthermore, the dynamic performance of the optimized 15 MW FOWT was investigated under normal and extreme environmental conditions. The mean drift forces affecting the wind turbine were analyzed after optimizing the floating foundation. The findings of this study can help to enhance the overall stability and dynamic performance of the 15 MW FOWT and contribute to its further optimization.

## 2. Materials and Methods

### 2.1. The Aerodynamic Loads

Blade element momentum (BEM) theory, which combines momentum theory and blade element theory, has been widely used for calculating induced velocities on the blades of wind turbines. The general principle of the theory is based upon empirical lift and drag coefficients, and forces are developed locally at the airfoil. The forces are balanced with the change in momentum of the air flowing through the rotor disk [20]. The thrust extracted by each rotor annulus of width  $dr$  is equivalent to [21]:

$$dT = 4\pi r \rho U_{\infty}^2 (1 - a) a dr \quad (1)$$

where  $dT$  is the thrust extracted by each rotor annulus of width  $dr$ ;  $r$  is local radius;  $\rho$  is the air density;  $U_{\infty}$  is the mean wind speed;  $a$  is the axial induction factor;  $dr$  is the blade element and annulus width.

BEM theory is invalid for induction factors greater than 0.4. The Glauert correction is used for large induction factors. For  $a > 0.4$ , the empirical thrust curve recommended by Burton was used [20]:

$$a = \frac{(C_T/F - C_{T1})}{C_{T2} - C_{T1}}(a_2 - a_1) + a_1 \tag{2}$$

$$F = \frac{2}{\pi} \cos^{-1}(e^{-f}) \tag{3}$$

$$f = \frac{B}{2} \frac{R - r}{2r \sin \phi} \tag{4}$$

where  $a_2 = 1.0$ ;  $C_{T2} = 1.82$ ;  $a_1 = 1.0 - 0.5\sqrt{C_{T2}}$ ;  $C_{T1} = 4a_1(1 - a_1)$ ;  $F$  is the Prandtl factor;  $B$  is the number of blades;  $R$  is the outer radius of the rotor;  $r$  is the local radius; and  $\phi$  is the angle made by the trailing vortices at the rotor plane.

### 2.2. The Hydrodynamic Loads

Potential flow effect [22] and viscous effect are both essential for determining wave-induced motion and loads on marine structures. For marine systems with large scales relative to wave parameters (wave height and wavelength), the potential flow effect is dominant, and the viscous effects can be negligible. For slender members with small dimensions within the marine structures, the viscous effect is very important and cannot be ignored when calculating hydrodynamic load.

For the columns and pontoons of the semi-submersible foundation considered in this paper, the hydrodynamic loads can be divided into the following parts [20]:

$$F_{total} = F_{FK} + F_S + F_R + F_D \tag{5}$$

where  $F_{total}$  is the hydrodynamic loads on the columns and pontoons;  $F_{FK}$  is the Froude-Krylov forces, including buoyancy forces;  $F_S$  is the diffraction forces;  $F_R$  is added mass and damping forces;  $F_D$  is the drag forces.

For the slender members such as cross braces, Morison’s equation [23] was used for calculating the hydrodynamic loads. The horizontal force  $dF$  on a strip of length  $dz$  on a vertical rigid circular cylinder can be written as:

$$dF = \rho \frac{\pi D^2}{4} dz C_M a_1 + \frac{\rho}{2} C_D dz |u|u \tag{6}$$

where  $dF$  is the horizontal force, with the direction of positive force as the wave propagation direction;  $u$  is the horizontal undisturbed fluid velocity at the midpoint of the strip;  $a_1$  is the horizontal undisturbed fluid acceleration at the midpoint of the strip;  $D$  is the cylinder diameter;  $C_D$  and  $C_M$  are the drag and mass coefficients, respectively, which must each be empirically determined;  $\rho$  is the mass density of the water.

The wave excitation loads acting on the marine structure can be described as involving three components: first-order wave loads oscillating with the wave frequencies, second-order mean-drift, slow-drift, and rapidly varying wave loads, as well as the higher-order ringing forces [24]. In addition to the first-order wave loads, the mean-drift wave loads were also considered in this investigation. Mean-drift wave loads are known to exert an effect on the motion of floating foundations [4], and the relevant calculation includes momentum conservation in the three horizontal degrees of freedom and direct pressure integration, according to HydroD instructions [25]. The equation of the direct pressure integration method is as follows [26]:

$$F_{mean} = \int_c (-\frac{\rho g}{2} \overline{z_r^2}) n_1 ds - \omega_e^2 M \overline{\eta_3 \eta_5} + \omega_e^2 M (\overline{\eta_2 - Z_G \eta_4}) \eta_6 + \rho \int_{S_B} \{ (\eta_2 + x \eta_6 - z \eta_4) \frac{\partial}{\partial y} (\frac{\partial \varphi^{(1)}}{\partial t} + U \frac{\partial \varphi^{(1)}}{\partial x}) \Big|_m + (\eta_3 - x \eta_5 + y \eta_4) \frac{\partial}{\partial z} (\frac{\partial \varphi^{(1)}}{\partial t} + U \frac{\partial \varphi^{(1)}}{\partial x}) \Big|_m + \frac{1}{2} ((\frac{\partial \varphi^{(1)}}{\partial x})^2 + (\frac{\partial \varphi^{(1)}}{\partial y})^2 + (\frac{\partial \varphi^{(1)}}{\partial z})^2) \} n_1 ds \tag{7}$$

where  $c$  is the waterline curve;  $\zeta_r = \zeta - (x\eta_3 + y\eta_4)$  is the relative wave amplitude along with the ship;  $\omega_e$  is encounter frequency;  $\phi^{(1)}$  is first-order velocity potential;  $\zeta_i (i = 1, 2, \dots, 6)$  is the displacement of the vessel in six degrees of freedom;  $S_B$  is the average wet surface of the body;  $M$  is the mass of the ship;  $Z_G$  is z-coordinate of the center of gravity of the ship;  $|_m$  indicates that the variables should be evaluated on the average position of the wet ship hull; the bar over the expressions indicates time-averaged values. It is feasible by this method to obtain the mean drift wave load for six degrees of freedom.

### 2.3. Equations of Motion

The kinetics for the foundation’s movement in water can be expressed as follows [24]:

$$\mathbf{V} \begin{bmatrix} v' \\ \omega' \end{bmatrix} + \begin{bmatrix} \omega \times P \\ \omega \times L + v \times P \end{bmatrix} = \begin{bmatrix} F_1 \\ M_1 \end{bmatrix} \tag{8}$$

$$F = F_1 + F_A \tag{9}$$

$$M = M_1 + M_A \tag{10}$$

where  $\mathbf{V}$  is the virtual-mass matrix,  $\mathbf{V} = \mathbf{A} + \mathbf{B}$ ;  $\mathbf{A}$  is the added-mass matrix;  $\mathbf{B}$  is the body-mass matrix;  $P$  is the virtual linear momentum,  $P = P_A + P_B$ ;  $P_A$  is the added linear momenta;  $P_B$  is the linear momentum;  $L$  is the virtual angular momentum,  $L = L_A + L_B$ ;  $L_A$  is the added angular momentum;  $L_B$  is the angular momentum;  $F$  is the external force;  $M$  is the external moment;  $F_A$  is the added inertia force;  $M_A$  is the added inertia moment;  $v$  is the velocity of the body origin;  $\omega$  is the angular velocity of body; Use of  $'$  denotes time derivatives with respect to the body-fixed system of reference.

In the time-domain analysis, the motion of the foundation [24] can be given by:

$$(\mathbf{m} + \mathbf{A}_\infty)\ddot{\mathbf{x}} + \mathbf{D}_1\dot{\mathbf{x}} + \mathbf{D}_2f(\dot{\mathbf{x}}) + \mathbf{K}\mathbf{x} + \int_0^t h(t - \tau)\dot{\mathbf{x}}(\tau)d\tau = \mathbf{q}(t, \mathbf{x}, \dot{\mathbf{x}}) \tag{11}$$

$$\mathbf{q}(t, \mathbf{x}, \dot{\mathbf{x}}) = \mathbf{q}_{WI} + \mathbf{q}_{WA}^{(1)} + \mathbf{q}_{WA}^{(2)} + \mathbf{q}_{CU} + \mathbf{q}_{ext} \tag{12}$$

$$h(\tau) = \frac{1}{2\pi} \int_{-\infty}^{\infty} \mathbf{c}(\omega) + i\omega\mathbf{a}(\omega)e^{i\omega\tau} d\omega \tag{13}$$

where  $\mathbf{m}$  is the body mass matrix;  $\omega$  is the angular frequency;  $\mathbf{A}_\infty$  is the frequency-dependent added-mass matrix when  $\omega = \infty$ ,  $\mathbf{A}(\omega) = \mathbf{A}_\infty + \mathbf{a}(\omega)$ ;  $\mathbf{x}$  is position vector, with the body initially located at the origin position of the global coordinate system. The x–y plane of the global coordinate system coincides with the calm water plane, and the z-axis is determined by the cross product of the x-axis and the y-axis. The translational motions of the body on the x-, y-, and z-axes are defined as surge, sway, and heave, respectively. The rotating motions around the x-, y- and z-axes are defined as roll, pitch, and yaw, respectively.  $\mathbf{K}$  is the hydrostatic stiffness matrix;  $\mathbf{D}_1$  is the linear damping matrix;  $\mathbf{D}_2$  is the quadratic damping matrix;  $h(\tau)$  is the retardation function computed by a transform of the frequency-dependent added-mass and damping;  $f$  is vector function where each element is given by  $f_i = \dot{x}_i|\dot{x}_i|$ ;  $\mathbf{C}_\infty$  is the frequency-dependent potential damping matrix when  $\omega = \infty$ , and  $\mathbf{C}(\omega) = \mathbf{C}_\infty + \mathbf{c}(\omega)$ ;  $\mathbf{q}(t, \mathbf{x}, \dot{\mathbf{x}})$  is the exciting force vector;  $\mathbf{q}_{WI}$  is the wind drag force;  $\mathbf{q}_{WA}^{(1)}$  is the first-order wave excitation force;  $\mathbf{q}_{WA}^{(2)}$  is the second-order wave excitation force;  $\mathbf{q}_{CU}$  is the current drag force;  $\mathbf{q}_{ext}$  is any other force.

### 2.4. Finite Element Formulation

The structural analyses of the mooring lines and tower in this study were carried out using the finite element method (FEM). This section presents the theoretical basis for the finite element formulation, constructed on the basis of the principles of continuum mechanics.

The motion of material particles, expressed by the Lagrangian description, was referred to a fixed global Cartesian coordinate frame defined by the base vectors  $\mathbf{I}_i, i = 1, 2$  or 3.

Each particle was identified by its position vector  $\mathbf{X}$  in an arbitrarily chosen reference configuration, which may be the initial configuration  $C_0$ . The motion of the particle can be described as [27]:

$$x = x(\mathbf{X}, t) \tag{14}$$

$$x = \mathbf{X} + \mathbf{u} \tag{15}$$

where  $x$  denotes the particle’s position at time  $t$ ;  $\mathbf{u}$  is the displacement vector.

For the Lagrangian formulation, the strains were measured in terms of the Green strain tensor  $\mathbf{E}$ . If  $C_0$  is used as reference configuration, this strain tensor is defined by [27]:

$$dS_n^2 - dS_0^2 = 2d\mathbf{X} \cdot \mathbf{E} \cdot d\mathbf{X} \tag{16}$$

where  $dS_0$  and  $dS_n$  denote the length of the line segment before and after deformation.

The symmetric Piola-Kirchhoff stress tensor  $\mathbf{S}$  referring to  $C_0$ , always used in conjunction with Green strain in the analysis, can be expressed as [27]:

$$\mathbf{S} = S_{ij}\mathbf{I}_i\mathbf{I}_j \tag{17}$$

where  $S_{ij}$  denotes the components of  $\mathbf{S}$  in the original coordinate frame  $\mathbf{I}_j$ .

In the following, on the basis of small strain theory, it is assumed that  $L_0$  is the initial stress-free element length. The axial force of the mooring line elements is given by [27]:

$$N = \frac{L - L_0}{L_0}(EA) \tag{18}$$

$$\varepsilon = \frac{L - L_0}{L_0} \tag{19}$$

where  $L_0$  is the initial stress-free element length;  $EA$  is the axial stiffness;  $\varepsilon$  is the strain.

### 2.5. Method of the Integrated Analysis of the FOWT

The integrated time-domain analysis of the whole floating wind turbine is was conducted in SIMA (SIMO/RIFLEX/AERODYN) [28]. The multiple physics engines in SIMA can calculate different loads on each part of the FOWT and combine them for the integrated dynamic analysis. The dynamic equilibrium [27] of the integrated FOWT model in SIMA can be expressed as follows:

$$\mathbf{R}^I(\mathbf{r}, \ddot{\mathbf{r}}, t) + \mathbf{R}^D(\mathbf{r}, \dot{\mathbf{r}}, t) + \mathbf{R}^S(\mathbf{r}, t) = \mathbf{R}^E(\mathbf{r}, \dot{\mathbf{r}}, t) \tag{20}$$

where  $\mathbf{R}^I$  is the inertia force vector;  $\mathbf{R}^D$  is damping force vector;  $\mathbf{R}^S$  is internal structural reaction force vector;  $\mathbf{R}^E$  is external force vector;  $\mathbf{r}$ ,  $\dot{\mathbf{r}}$ , and  $\ddot{\mathbf{r}}$  are the structural displacement, velocity, and acceleration vectors. The external force vector includes weight and buoyancy, forced displacements due to floating foundation motions, drag and wave particle acceleration terms in the Morison equation, and specified discrete nodal point forces.

The inertia force vector can be expressed as:

$$\mathbf{R}^I(\mathbf{r}, \ddot{\mathbf{r}}, t) = [\mathbf{M}^S + \mathbf{M}^F(\mathbf{r}) + \mathbf{M}^H(\mathbf{r})]\ddot{\mathbf{r}} \tag{21}$$

where  $\mathbf{M}^S$  is the structural mass matrix;  $\mathbf{M}^F(\mathbf{r})$  is mass matrix accounting for internal fluid flow;  $\mathbf{M}^H(\mathbf{r})$  is the displacement-dependent hydrodynamic mass matrix accounting for the structural acceleration terms in the Morison equation as added mass contributions in local directions.

The damping force vector is described by:

$$\mathbf{R}^D(\mathbf{r}, \dot{\mathbf{r}}) = [\mathbf{C}^S(\mathbf{r}) + \mathbf{C}^H(\mathbf{r}) + \mathbf{C}^D(\mathbf{r}, \dot{\mathbf{r}})]\dot{\mathbf{r}} \tag{22}$$

Where  $C^S(\mathbf{r})$  is the internal structural damping matrix;  $C^H(\mathbf{r})$  is the hydrodynamic damping matrix accounting for diffraction effects for floating or partly submerged elements (irrelevant in other situations);  $C^D(\mathbf{r}, \dot{\mathbf{r}})$  is the matrix of specified discrete dashpot dampers which may be dependent on displacement and velocity.

### 3. Numerical Model

A numerical model of an integrated large-scale floating wind turbine was established, composed of four main parts: the rotor, the tower, the floating foundation, and the mooring lines. This section details the parameter information for each part of the floating wind turbine. The rotor, tower, and mooring lines of the wind turbine were established as finite element models. The dynamic forces acting on them in the time domain were analyzed according to the BEM and FEM methods, respectively. The floating foundation of the wind turbine was established with the panel model and the Morison model, and the hydrodynamic performance of the foundation was calculated based on potential flow theory and the Morison equation.

#### 3.1. 15 MW Wind Turbine and Tower

The 15 MW reference wind turbine model [29] provided by the NREL is referred to in this paper. The rotor diameter of the wind turbine is 240 m, and the hub height is 150 m. The blades of the wind turbine consist of eight types of airfoils, as shown in Figure 1. The wind turbine adopts the direct-drive layout for its nacelle. The maximal rotor speed can reach 7.56 rpm. The controllers of the generator torque and blade pitch are designed to maintain stable output power. The detailed properties of the wind turbine are shown in Table 1.

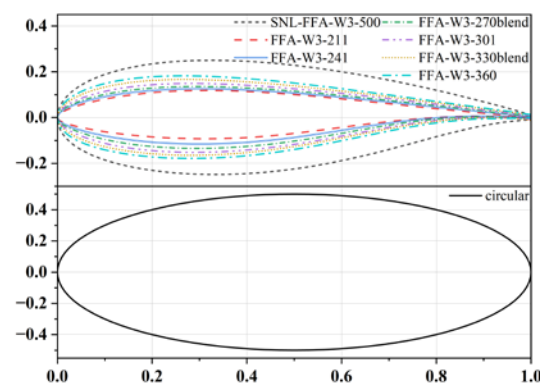


Figure 1. Airfoil data for the blades.

Table 1. Parameters of the 15 MW reference wind turbine.

Parameter	Value
Power rating	15 MW
Number of blades	3
Cut-in wind speed	3 m/s
Rated wind speed	10.59 m/s
Cut-out wind speed	25 m/s
Rotor diameter	240 m
Hub height	150 m

In the model, the whole tower height of the wind turbine was about 130 m, and the height of the tower base from the still water line (SWL) was 15 m. The outer diameter at the tower base was 10 m, and the outer diameter at the top was 6.5 m.

### 3.2. The Semi-Submersible Floating Foundation

In deep water, a floating foundation is generally used to support the superstructure (including the rotor and tower). The University of Maine (UMaine) VoltturnUS-S reference foundation was considered in this study [17]. It is composed of three outer columns, a central column, and three rectangular pontoons at the bottom, as shown in Figure 2. The outer columns are connected to the central column via three cross braces at the top of the columns, making the overall structure relatively stable. The three bottom pontoons are attached to the bottom of the columns, respectively. The overall height of the foundation is 35 m, with a draft of 20 m and a freeboard of 15 m, and the maximum width is 102.13 m. The detailed parameters of the floating foundation are shown in Table 2.

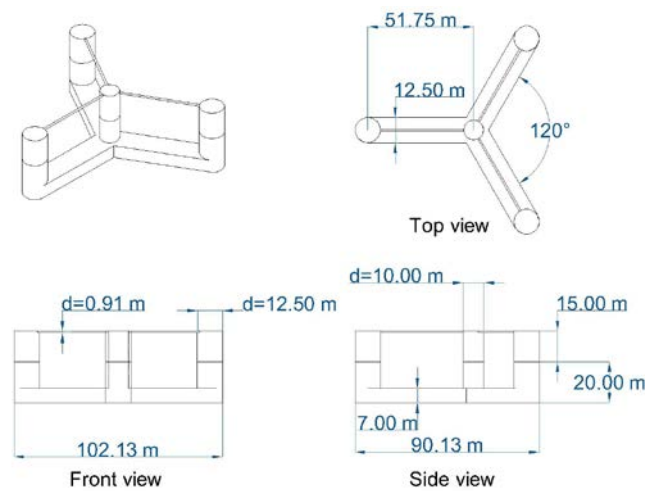


Figure 2. Detailed dimensions of the semi-submersible foundation.

Table 2. Properties of the semi-submersible foundation.

Parameter	Value
Foundation type	Semi-submersible
Hull Displacement	20,206 m <sup>3</sup>
Draft	20 m
Freeboard	15 m
Vertical Center of Gravity from SWL	−14.94 m
Vertical Center of Buoyancy from SWL	−13.63 m
Roll Inertia about Center of Gravity	1.251 × 10 kg·m <sup>2</sup>
Pitch Inertia about Center of Gravity	1.251 × 10 kg·m <sup>2</sup>
Yaw Inertia about Center of Gravity	2.367 × 10 kg·m <sup>2</sup>

### 3.3. The Mooring System

A chain catenary mooring system can constrain the movement of the floating foundation and improve the stability of the foundation under the action of wind and waves. For the catenary part of the mooring lines, the heave motion of the foundation can to a certain extent be reduced due to the weight of the catenary equipment. The friction between the lying cable and the seabed can decrease the displacement amplitude of the foundation. Furthermore, the deviation of the foundation from its equilibrium position can be limited by the axial stiffness of the mooring lines. In this paper, a three-line chain catenary mooring system [17] at a depth of 200 m was considered, and the unstretched length of the mooring lines was 850 m. The anchors were spaced equally at 120 degrees between every two anchors, radially, at 837.60 m from tower’s centerline. Further properties of the mooring system are listed in Table 3, and the specific arrangement of the mooring system is illustrated in Figure 3.

**Table 3.** Properties of the mooring system.

Parameter	Value
Mooring System Type	Chain Catenary
Line Breaking Strength	22,286 kN
Depth of Anchor	200 m
Depth of Fairlead	14 m
Radial Spacing of Fairlead	58 m
Nominal Chain Diameter	0.185 m
Dry Line Linear Density	685 kg/m
Extensional Stiffness	3270 MN
Unstretched Length of Line	850 m

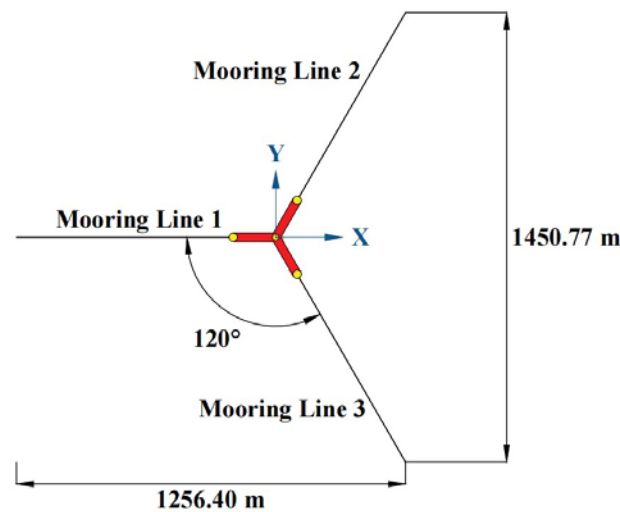


**Figure 3.** Arrangement of the mooring system.

3.4. Convergence Study of the Floating Foundation Mesh

Based on potential flow theory and the Morison equation, the columns and pontoons of the floating foundation were modelled in HydroD as the panel, and the cross braces were established according to the Morison model. The hydrodynamic model was divided into boundary element meshes to conduct the hydrodynamic analysis. In order to ensure the accuracy of the calculation, the hydrodynamic models with different mesh densities were processed in GeniE [30], as shown in Table 4, and the convergence study of the meshes was carried out.

**Table 4.** The different mesh models of the floating foundation.

	The Size of the Mesh Elements	Mesh Number of the Panel Model	Mesh Number of the Morison Model
Model 1	0.75 m × 0.75 m	20,971	162
Model 2	1.0 m × 1.0 m	11,291	123
Model 3	1.25 m × 1.25 m	7353	99
Model 4	1.5 m × 1.5 m	5525	81

The results of the convergence study were obtained by comparing the motion and wave excitation load transfer functions of different mesh models for the same wave direction, as presented in Figure 4; the horizontal axis represents the different wave periods, and the vertical axis the motions and wave excitation forces of the floating foundation. The legends in Figure 4 correspond to the different mesh models shown in Table 4. The terms “Force 1” and “Force 3” denote first-order wave excitation forces on the floating foundation in the surge and heave directions, respectively, and “Force 5” denotes first-order wave excitation moments in the pitch direction. It can be found from Figure 4d–f that the first-order

wave excitation load transfer functions of the four mesh models were basically the same, indicating that accurate calculation of first-order wave excitation loads can be obtained by any of the four mesh models.

However, within the calculations of the four mesh models, some deviations around the peak values of the surge and pitch transfer functions were observed, as in Figure 4a,c. This suggests that coarser meshes, such as Model 4, were unable to capture accurately the variations of the floating foundation’s motion, resulting in underestimation of the surge and pitch motion. A similar phenomenon occurred in the heave transfer function at the 20 s wave period, as shown in Figure 4b, suggesting that coarser meshes can also influence the accuracy of the heave transfer function. Therefore, it was considered that a denser mesh model will lead to more accurate hydrodynamic data, and Model 1 was used for the subsequent hydrodynamic analysis, performance optimization, and time-domain dynamic analysis, as shown in Figure 5.

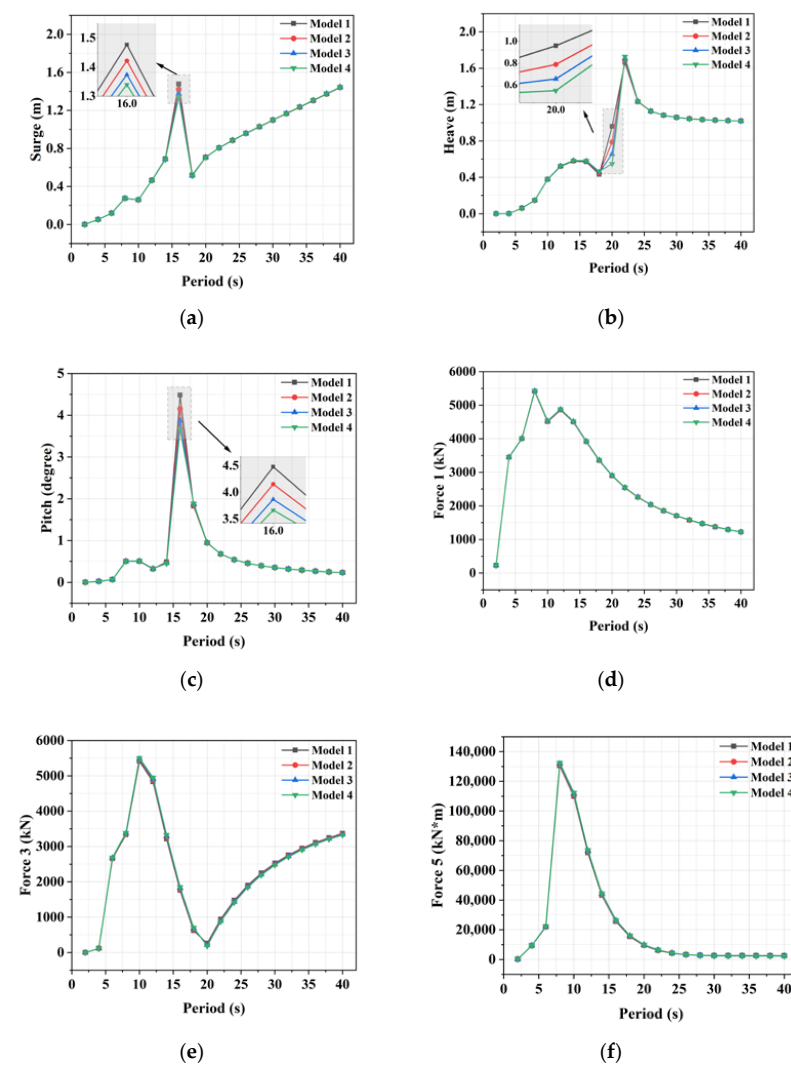


**Figure 4.** The comparison of the RAOs of the different mesh models in the 0-degree wave direction: (a) RAOs of surge motion; (b) RAOs of heave motion; (c) RAOs of pitch motion; (d) RAOs of Force 1; (e) RAOs of Force 3; (f) RAOs of Force 5.

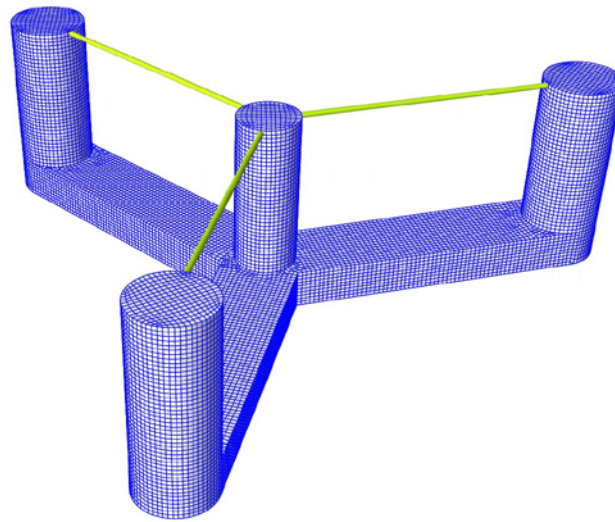


Figure 5. Image of Model 1.

3.5. The Verification of the Hydrodynamic Data

For the accuracy of the subsequent numerical simulation, it was necessary to conduct verification of the hydrodynamic data. This study calculated the hydrodynamic coefficients of the floating foundation, using WADAM [31]. First-order wave excitation loads from WADAM were compared in the same wave direction with the reference data from WAMIT [32] provided by the NREL [17], and the results are illustrated in Figure 6. For brevity, the comparisons of the wave excitation forces in three different degree-of-freedom directions are all shown in the same graph. There are three colors in Figure 6; the axes, titles, and curves of the same color represent information on the wave excitation forces in each of the three directions. The horizontal axes show different wave periods and the vertical axes show the magnitude of the excitation force. The different colored curves indicate wave excitation loads for different degrees of freedom, corresponding to the same colored horizontal and vertical axes. The red curves represent the wave excitation loads in the vertical direction, and the blue curves represent the wave excitation moments about the y axis. The legend of Figure 6 shows the results from WAMIT and WADAM. The terms “Force 1”, “Force 3”, and “Force 5” have the same meaning as above. It can be seen that the first-order wave excitation loads calculated in WADAM well matched the reference data in the three-degrees-of-freedom direction, proving that the assessment of the hydrodynamic performance of the floating foundation in this paper is reliable.

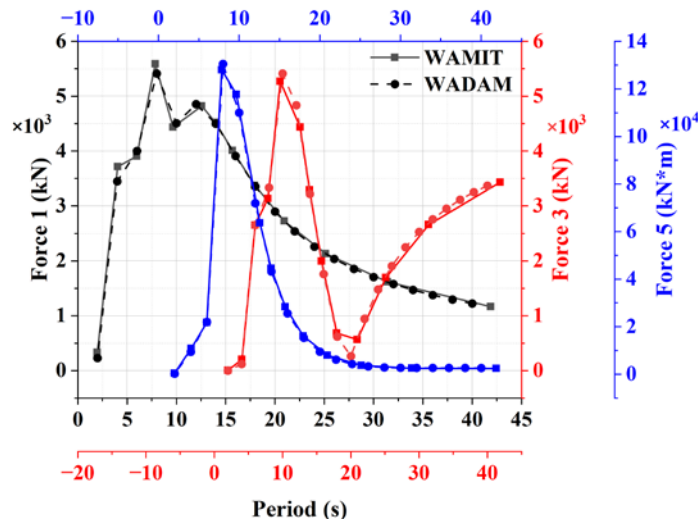


Figure 6. Comparison of the first-order wave excitation loads from WADAM and WAMIT.

Subsequently, the floating foundation model was combined with the numerical models of the rotor, tower, and mooring system in SIMA to construct an integrated 15 MW FOWT, as shown in Figure 7.

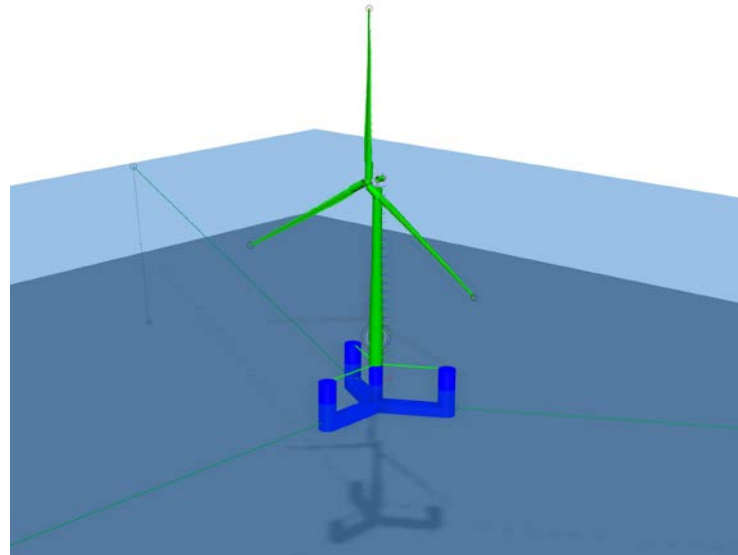


Figure 7. Image of the combined 15 MW FOWT numerical model.

### 3.6. Environmental Condition

This study established two environmental conditions, details of which are shown in Table 5. For the “EC1” condition, referring to the wave parameters of the South China Sea stated in [33], the floating wind turbine was in normal operation when the average speed of the turbulent wind equal to the rated wind speed. The “EC2” condition was an extreme sea condition with a 100-year return period, the parameters of which are described in DNV-OS-E301 [34], and the wind turbine was in a shutdown state.

Table 5. Specific details of environmental conditions.

Environmental Condition	Wave Spectrum	Significant Wave Height	Peak Wave Period	Wind Spectrum	Wind Speed
EC1	Jonswap	0.5 m	4.5 s	NPD	10.59 m/s
EC2	Jonswap	7.3 m	11.1 s	NPD	28.6 m/s

## 4. Results and Discussion

In order to improve the hydrodynamic performance of the large floating offshore wind turbine (FOWT), this paper investigated the influence on the hydrodynamic performance of the floating foundation of two structural parameters: the distance between the outer columns and the central column, and the diameter of the outer columns. The structure of the floating foundation was optimized based on the findings

### 4.1. The Effect of the Distance between the Outer Columns and the Central Column

In this study, the distance between the outer columns and the central column of the floating foundation was changed, and the motion and wave excitation force transfer functions of floating foundations with different column spacing were calculated, to investigate the effect of column spacing on the hydrodynamic performance of the foundation. Other structural parameters of the floating foundation remained unchanged, and the original column spacing of the foundation was 51.75 m. The distance between the outer columns and central column was set to vary by every 2.5% within the range of 90% to 110% of its original design value. The motion and wave excitation force transfer functions were calculated for the floating foundations with changed column spacing.

The motion transfer functions of the foundations with different column spacing in the 0-degree wave direction are depicted in Figure 8. The horizontal axis in Figure 8 represents the different wave periods, and the vertical axis denotes the motion amplitude of the floating foundation. Curves with different colors and symbols are used in Figure 8 to represent the motion transfer functions of the floating foundations with different column spacing. For example, the black line with the square symbol in Figure 8a shows the surge transfer function in the 0-degree wave direction for the foundation with 90% of the original design value for its column spacing.

Due to limited space in this paper, the transfer functions of surge, heave, and pitch motions were selected for analysis. Figure 8 indicates that, for the UMaine VoltturnUS-S reference semi-submersible foundation, column spacing had a significant effect on motion transfer functions. The peak values of different surge and pitch transfer functions were all located around the position of the 16 s wave period. However, with the changes to column spacing, the peak values of the surge and pitch transfer functions showed obvious variation, as indicated in Figure 8a,c. This indicates that the variation of the column spacing can change the amplitudes of the surge and pitch resonance motions. In addition, the wave period corresponding to the peak value of heave transfer function also changed with the continuous increase of column spacing, as shown in Figure 8b.

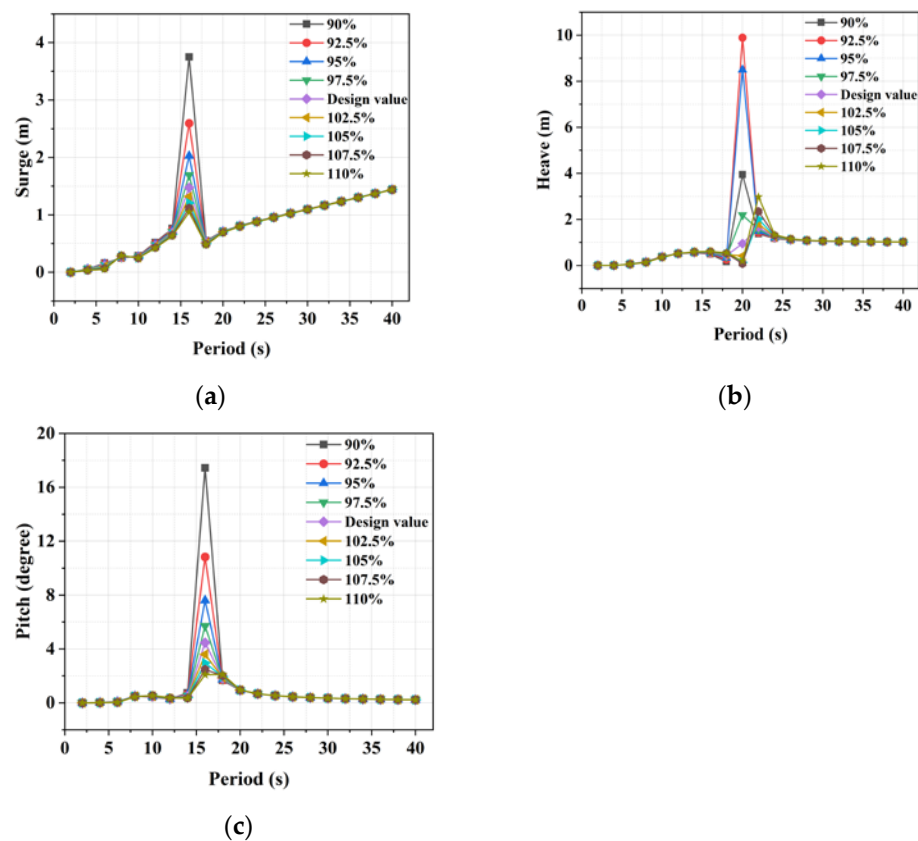


**Figure 8.** Motion transfer functions of the floating foundation with different column spacings: (a) Transfer function of surge motion; (b) transfer function of heave motion; (c) transfer function of pitch motion.

The peak values of those transfer functions were analyzed, and the results are shown in Figure 9. The horizontal axis of Figure 9 indicates the different column spacing, and the vertical axis represents the magnitude of the peak values for the transfer functions. The black solid lines in Figure 9 give the variation curves of the peak motion transfer function values with the change of column spacing, and the magnitude of the peak value is indicated by the black vertical axis on the left side of the plot. The red dotted lines represent the

variation curves of the peak values for the wave excitation load transfer functions, and the magnitude of the peak values is shown by the red vertical axis on the right side of the diagram. The curves with different symbols represent the variation curves of the peak values for transfer functions in different wave directions. For example, the black solid line with the square symbol in Figure 9c represents the variation curve of the peak value for surge transfer function with the change of column spacing in the 0-degree wave direction. The red dotted line with the circular symbol represents the variation curve of the peak value of the longitudinal wave excitation moment transfer function with the change of column spacing in a 60-degree wave direction.

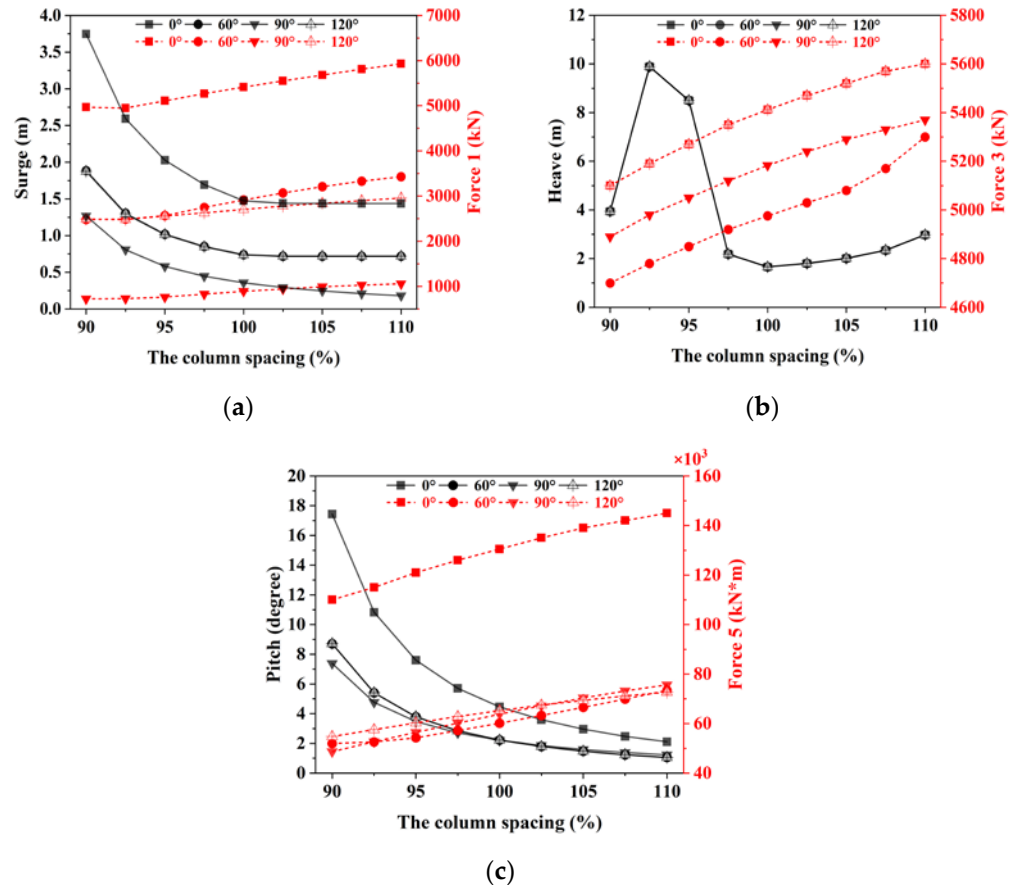


**Figure 9.** The peak values of the transfer functions with different column spacing in the different wave directions: (a) Peak values of surge motion and Force 1 transfer functions; (b) peak values of heave motion and Force 3 transfer functions; (c) peak values of pitch motion and Force 5 transfer functions.

It can be seen from Figure 9 that the change of column spacing significantly affected the motion and wave excitation loads of the floating foundation. In all four wave directions, the peak values of surge and pitch motion transfer functions decreased with the increase of column spacing, and the wave excitation force and moment on the foundation in the longitudinal direction increased gradually, as shown in Figure 9a,c. This is because the increase of the distance between the columns caused a rise in the longitudinal inertia moment of the floating foundation, which increased the restoring moment of the foundation and strengthened the ability to return to its equilibrium position under the action of the wave. On the other hand, the pontoons of the floating foundation were longer due to the larger column spacing, which prompted an increase in the displacement of the foundation. These two factors reduced the peak value of the motion transfer function for the same wave action. In other words, within a certain range, increased column spacing can reduce the amplitude of resonant motion that occurs when the wave frequency is close to the natural frequencies of the surge and pitch motions of the floating foundation. However, owing to

increased column spacing, the dimensions of the floating foundation were larger, making the wave excitation force on the foundation more significant.

Furthermore, the influence of column spacing on the peak value of the heave motion transfer function was also found to be significant. Within the variation range of the column spacing selected in this paper, when the distance between the outer columns and the central column was 92.5% of the original design value, the peak value of the heave motion transfer function was the largest. Moreover, the wave excitation force experienced by the floating foundation in the vertical direction can also be increased by the larger column spacing.

The peak value curves of surge and pitch transfer functions varied within a similar trend for different wave directions, as can be seen in Figure 9a,c. However, for the surge and pitch transfer functions, the peak value curves at the 0-degree wave direction were higher overall than those under other wave directions. With the change of wave direction from 0 to 90 degrees, the surge and pitch motions of the foundation become smaller, and the peak value curves under 90-degree wave direction were lower overall than the others. This shows that the floating foundation will generate the largest motion when the wave direction is close to the direction of motion. In addition, the difference in the peak values of the heave transfer functions was small under different wave directions, as shown in Figure 9b, indicating that the change of wave direction had little effect on heave motion.

Based on the above research results on the influence of column spacing on hydrodynamic performance, the structural parameters of the floating foundation were optimized. To reduce the motion responses under the action of the wave and to improve the hydrodynamic performance of the foundation, its column spacing was increased by 5% of the original design value, i.e., 54.3375 m. In the case of the 90-degree wave direction, for the optimized floating foundation, the peak value of the surge transfer function was reduced by 30.85% of the original. Under the condition of the 0-degree wave direction, the peak value of the pitch transfer function of the optimized floating foundation was reduced by 33.61% compared with the original. For the roll transfer function, the peak value of the optimized foundation for a 90-degree wave direction was 35.45% lower than that of the original model.

#### 4.2. The Effect of the Diameter of the Outer Columns

According to the above results, the effect of the column diameter on the hydrodynamic performance was studied, based on the above optimized floating foundation, to facilitate the further performance optimization of the foundation. The investigation into the influence of the column diameter on the hydrodynamic performance adopted the same method as above. Other structural parameters of the foundation were kept unchanged, and the column diameter was changed with a step size of 2.5% within the range of 90% to 110% of the design value of the outer column diameter. The hydrodynamic data were calculated for the floating foundation with different outer column diameters. The transfer functions of the motion and wave excitation forces were analyzed, as shown in Figure 10. Curves with different colors and symbols are used in Figure 10 to represent the motion transfer functions for the floating foundations with different outer column diameters.

From Figure 10, it can be seen that the peak value of the surge transfer function was significantly affected by the change of the outer column diameter, and the change of the outer column diameter had little effect on the heave transfer function, as shown in Figure 10a,b. This indicates that the change of the outer column diameter to some extent helped to reduce the surge resonance of the floating foundation when the wave frequency was close to the natural surge frequency. The heave motion was apparently not altered by the change of column spacing. In addition, the peak value of the pitch transfer function was significantly affected by the variation of the outer column diameter. When the diameter of the outer column was changed to a specific value, a new peak value was generated in the pitch transfer function. In other words, the variation of the outer column diameter not only influenced the amplitude of the pitch resonance, but may also change the natural pitch frequency of the floating foundation.

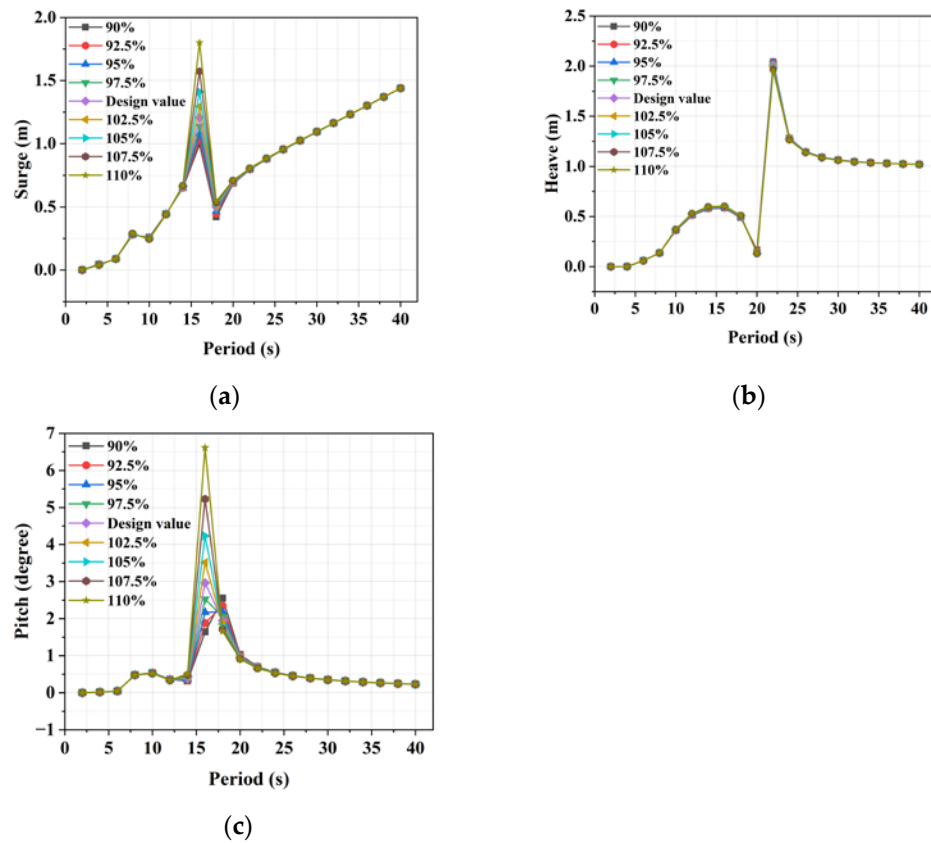


**Figure 10.** The motion transfer function of the optimized floating foundation with different column diameters: (a) Transfer function of surge motion; (b) transfer function of heave motion; (c) transfer function of pitch motion.

On the basis of the above analysis of the RAOs, it can be seen that waves in the period of 14–24 s caused severe resonance motion in the floating foundation. Therefore, the most frequent wave period occurring in the sea where the FOWT is located should be outside this range. Moreover, waves with a period of about 16 s can easily cause surge and pitch resonance motion within the foundation, resulting in very large longitudinal displacement and pitch angle. The amplitude of surge and pitch resonance motion can be reduced by changing the column spacing and the diameter of the outer column appropriately.

Figure 11 presents the peak values of the motion and wave excitation force transfer functions of the floating foundation with different column diameters in different wave directions. The black solid lines in Figure 11 are the variation curves of the peak values for the motion transfer functions with the change of outer column diameter, and the magnitude of the peak value shown by the black vertical axis on the left side of the plot. The blue dotted lines represent the variation curves of the peak values for the wave excitation load transfer functions, and the magnitude of the peak values is indicated by the blue vertical axis on the right side of the diagram. The curves with different symbols represent the variation curves of the peak values for the transfer functions in different wave directions.

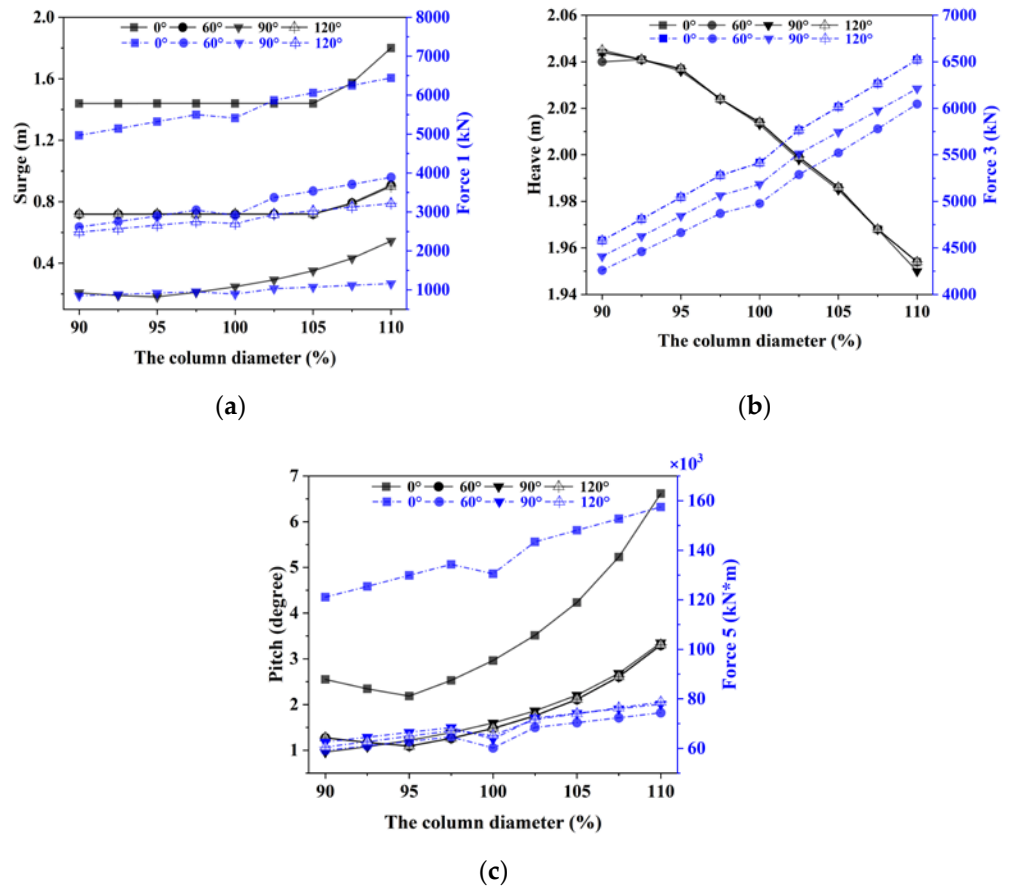


**Figure 11.** The peak values of the transfer functions with different column diameters in the different wave directions: (a) Peak values of surge motion and Force 1 transfer functions; (b) peak values of heave motion and Force 3 transfer functions; (c) peak values of pitch motion and Force 5 transfer functions.

It can be seen from Figure 11 that the peak values of the wave excitation force transfer functions were larger with the increase of the column diameter. Variation of the outer column diameter can lead to changes in the water-plane area and the displacement volume of the foundation; the smaller the column diameter, the smaller the water-plane area and the displacement volume become. The restoring moment of the floating foundation was affected by the change of the water-plane area and the displacement volume. From the results in Figure 11c, it can be seen that with the increase of column diameter, the peak values of the pitch transfer function became gradually larger. This indicates that the reduction of the column diameter increased the longitudinal restoring moment of the floating foundation, thereby decreasing the amplitude of the pitch resonance motion. In this study, for the case of 0-degree wave direction, the amplitude of the pitch resonance motion was smallest when the outer column diameter was 95% of the original design value. Under the effect of change in column diameter, the variation trend of the peak value of the roll transfer function was similar to that of the pitch transfer function. In contrast, for the heave transfer functions of the foundations, the peak value in all four wave directions decreased with the increase of column diameter. However, the magnitude of the change was small, reflecting that the change of the column diameter had limited influence on the heave motion.

In addition, within the variation range of the column diameter studied in this paper, the effect of the diameter change on the peak value of the surge transfer function was also limited. However, with the continuous increase of the column diameter, the peak value showed an apparent upward trend. Specifically, for the variation range of the column diameter smaller than the original design value, the change had little effect on the peak

value of the surge transfer function. However, within the range of column diameter larger than the original design value, the increase made the peak value of the surge transfer function more significant. The influence of column diameter variation on the peak value of the sway transfer function was similar to that for the surge transfer function.

Based on the above results, the floating foundation was further optimized. The outer column diameter of the final optimized foundation was reduced by 5% of the original design value. The initial design value of the outer column diameter was 12.5 m, and the outer column diameter of the final optimized foundation was 11.875 m. The hydrodynamic performance of the final optimized foundation was greatly improved in pitch and roll motion. In the 90-degree wave direction, for the final optimized floating foundation, the peak value of the surge transfer function was reduced by 26.58% compared with the previous optimized foundation. For the pitch transfer function of the final optimized foundation, the peak value in the 0-degree wave direction was 26.27% lower than that of the previous optimized foundation. As for the roll transfer function of the final optimized foundation, compared with the previous optimized foundation, the peak value was reduced by 26.12% in the 60-degree wave direction.

#### 4.3. The Performance Analysis of the Final Optimized Floating Foundation in the Time Domain

In this study, the final optimized floating foundation model was combined with the superstructure of a 15 MW wind turbine, and the time-domain dynamic performance of the integrated wind turbine was analyzed for two sea states. The total duration of the time-domain simulation was 2000 s. For the purpose of eliminating unstable numerical simulations, the results of the first 500 s were not considered. The analysis investigated the motion of the wind turbine with the optimized foundation in different sea conditions, the tension of the windward mooring line, and the mean drift forces on the foundation. Then, the results were compared with those of the wind turbine with the original UMaine VoltturnUS-S reference foundation.

Figure 12 presents the surge response of the wind turbine in the time domain for the two sea states before and after optimization of the floating foundation. Under EC1 conditions, when the wind turbine was operating normally, the extreme values of the surge response of the wind turbine were significantly reduced after the floating foundation was optimized. In the time-domain simulation for the wind turbine with the optimized foundation, the maximum surge motion was 3.80% lower than that of the wind turbine with the original foundation, and the standard deviation of the surge response was reduced by 19.78%. This demonstrates that the surge motion of the optimized wind turbine was more moderate.

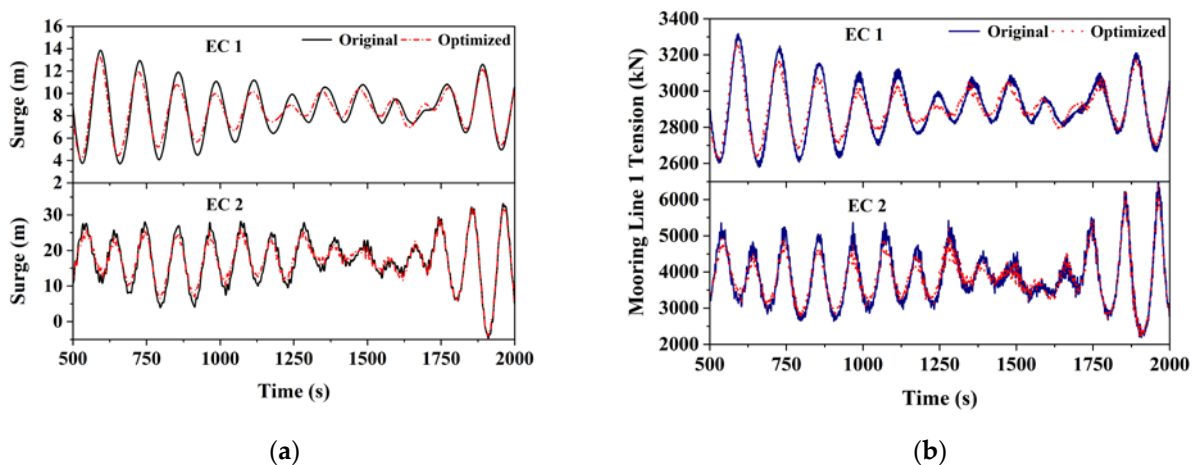


Figure 12. (a) The surge responses of the two wind turbines in two sea conditions in the time domain; (b) the ML1 tension for the two wind turbines in two sea conditions in the time domain.

The 15 MW wind turbine was shut down due to the high wind speed under EC2 conditions. Due to the high wind speed in extreme sea conditions, the aerodynamic load on the wind turbine was much larger than the wave load, and the optimization of the floating foundation had a relatively weak effect on the motion response of the integrated wind turbine. After the floating foundation was optimized, the maximum value of the surge response of the wind turbine was reduced by 2.78%, and its standard deviation was reduced by 13.31%.

In this study, under the combined action of wind and wave, the first mooring line (ML1) played a significant role in restricting the movement of the floating wind turbine and ensuring its stability. For the optimized floating wind turbine, the tension of the ML1 reduced with the decrease in the surge response, as shown in Figure 12b. Under EC1 conditions, the maximal tension of the ML1 of the wind turbine with the optimized foundation was reduced by 13.55%, and the standard deviation was reduced by 19.92% compared with the wind turbine with the original floating foundation. Under EC2 conditions, the maximum ML1 tension of the optimized wind turbine was reduced by 5.08%, and the standard deviation was reduced by 14.25%. This shows that the optimization of the floating foundation had a significant effect on decreasing the tension of the mooring line.

In addition, the optimization of the floating foundation also mitigated the sway, pitch, roll, and yaw motions of the wind turbine in the time-domain simulation. Under EC1 conditions, the standard deviation of the sway response of the optimized wind turbine was reduced by 12.61%. For the pitch response, after optimization of the foundation, the maximum value of the wind turbine in the time domain decreased by 2.08% under EC1 conditions. For the optimized floating wind turbine, the standard deviation of the roll response decreased by 20.95% under EC2 conditions, and the mean value of the yaw response was reduced by 4.74% under EC1 conditions.

The mean-drift force of the optimized floating wind turbine was also studied. Figure 13 shows the mean value and maximum value of the mean-drift force experienced by the wind turbines with the original and optimized floating foundations in different sea conditions. In Figure 13, the horizontal axis represents the maximum and mean values of the mean-drift forces on the FOWT under the two environmental conditions in the time domain simulation. The bar with diagonal lines in the legend indicates the statistical values of the mean-drift forces generated by the optimized FOWT, and the bar without patterns inside indicates the statistical value of the mean-drift forces on the original FOWT before optimization. The orange bars represent the statistical values of the mean-drift forces to which the two FOWTs were subjected under EC2 conditions, the magnitude of which is indicated by the orange vertical axis on the right side of the figure. The blue bars represent the statistical values of the mean-drift forces on the two FOWTs under EC1 conditions, the magnitude of which is shown in the blue vertical axis on the left side of the figure. For example, in Figure 13a, the leftmost blue bar without patterns inside shows the maximum value of the mean-drift forces on the original FOWT under EC1 conditions in the time domain simulation; the rightmost orange bar with diagonal lines represents the mean value of the mean-drift forces on the optimized FOWT under EC2 conditions.

Compared with the wind turbine on the original foundations, it can be observed that the mean and maximum values of the longitudinal force and moment on the wind turbine were each reduced after optimization of the foundation, as shown in Figure 13a,c. After the floating foundation was optimized, the maximum and mean values of the longitudinal force decreased by about 7.75% under EC1 conditions. For the 15 MW wind turbine with the optimized foundation under the EC2 conditions, the maximum value of the longitudinal moment was reduced by 11.68%, and the mean value was 13.43% lower than that of the wind turbine with the original foundation. However, in both EC1 and EC2 conditions, the vertical force on the wind turbine using the optimized foundation showed little increase compared with that on the original foundation, as shown in Figure 13b.

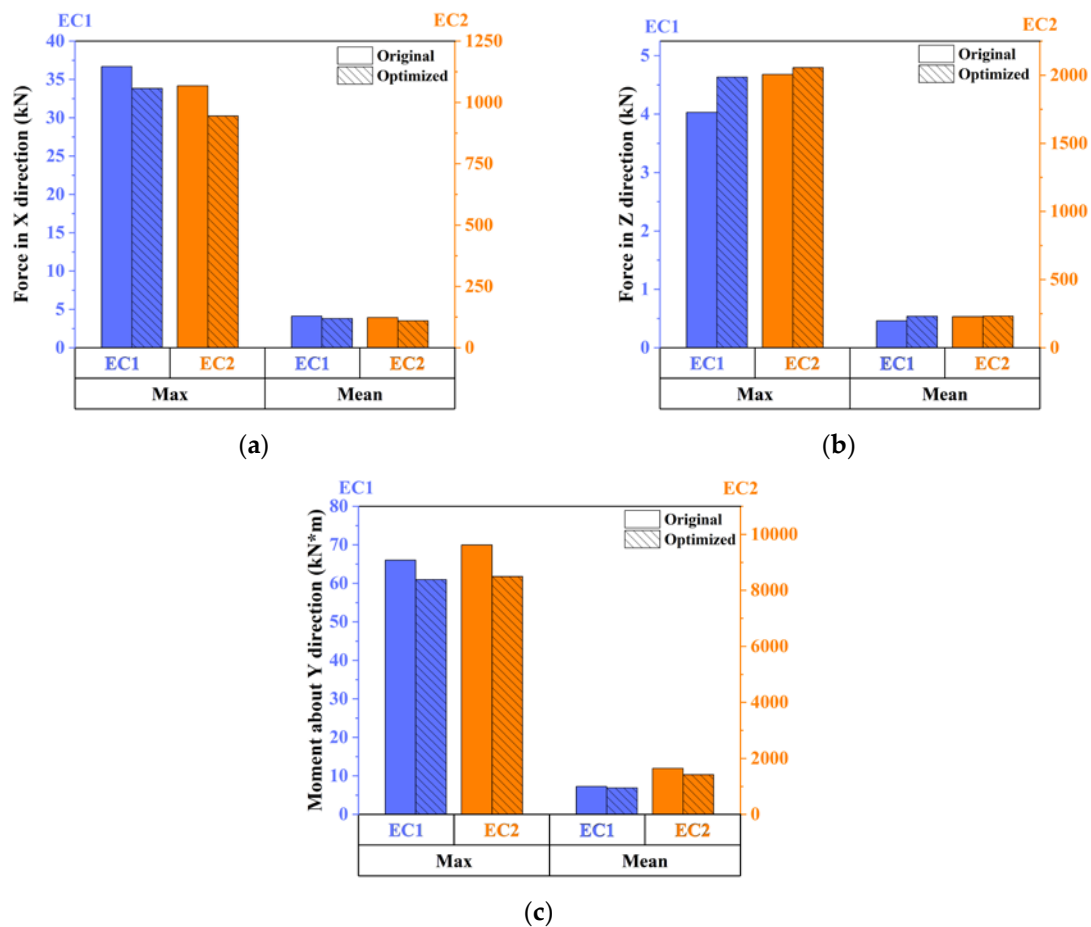


**Figure 13.** The statistics of the mean drift forces experienced by the two wind turbines under two environmental conditions: (a) The force in the X direction; (b) the force in Z direction; (c) the moment about Y direction.

### 5. Conclusions

The structural parameters of the UMaine VoltturnUS-S reference floating foundation are studied in this paper. The structural parameters of the floating foundation were considered in changes with a step size of 2.5% within the range of 90% to 110% of the design value. This study investigated the effects of the distance between the central column and the outer columns, as well as the diameter of the outer column, on the hydrodynamic performance of the floating foundation. Based on those results, the UMaine floating foundation was optimized and coupled with the 15 MW wind turbine. The dynamic performance of the optimized integrated FOWT was analyzed under normal and extreme conditions in the time domain, and compared with the FOWT using the original floating foundation model. The meaningful conclusions are as follows:

1. Within the variation range of column spacing studied in this paper, the change in column spacing had a significant influence on the hydrodynamic performance of the floating foundation. For the motion of the foundation, the increase of column spacing decreased the peak value of the surge transfer function. Since the inertia moment of the foundation became larger with the increase of column spacing, the restoring moment of the foundation also increased. At the same time, due to the increase of the column spacing, the pontoons of the foundation became longer, leading to an increase of the displacement volume of the foundation. These two factors eventually reduced the peak value of the pitch transfer function. In other words, the increase of column spacing can effectively mitigate the amplitude of the resonance motion when the wave frequency approaches the natural surge and pitch frequencies. The

- heave motion can also be affected by the change in column spacing. In the variation range of the column spacing, the peak value of the heave transfer function was the largest when the column spacing was 92.5% of the original design value. In addition, the peak value of the transfer function for the wave excitation force on the floating foundation increased with the increase of column spacing;
2. The change in the outer column diameter also significantly affected the hydrodynamic performance of the foundation. For the range of column diameters studied in this paper, with the continuous increase of the outer column diameter, the peak value of the surge transfer function appeared to demonstrate an obvious upward trend. The peak value of the heave transfer function decreased with the increase of the column diameter, but the overall variation of amplitude was small. The change of column diameter had a great impact on the pitch response of the foundation. A larger column diameter enlarged the water-plane area and the displacement volume of the floating foundation, which affected the restoring moment of the floating foundation. From the results of this paper, it appears that the increase of column diameter resulted in a relative decrease of the longitudinal restoring moment for the floating foundation, thereby increasing the peak value of the pitch transfer function. It can be seen that the reduction of the column diameter can moderate the pitch resonance motion of the floating foundation;
  3. Based on the results of the investigation into the structural parameters of the floating foundation, this study selected an optimization scheme for the foundation, with the column spacing increasing to 105% of the original design value and the diameter of the outer column decreasing by 5% compared with the original design value. After combining the optimized foundation with the 15 MW wind turbine, and comparing it with the wind turbine on the original foundation, it was found that the surge motion of the optimized wind turbine can be mitigated under normal conditions. In extreme conditions, the optimization of the foundation played a relatively weak role due to the tremendous aerodynamic load. After the optimization of the foundation, the sway, pitch, roll, and yaw motions of the floating wind turbine were also reduced to varying degrees. In particular, for surge responses under normal operating conditions, the standard deviation was reduced by 19.78% after optimization of the foundation. The tension of the mooring line on the optimized wind turbine was also reduced, as a result of the more moderate surge motion. In addition, the longitudinal mean-drift force and moment suffered by the wind turbine were also decreased owing to the optimization of the floating foundation.

This paper aimed to study the influence of structural parameters on the hydrodynamic performance of the UMaine VoltturnUS-S reference floating foundation. Other parameters (including draft) remained unchanged while the column spacing and the outer column diameters were changed during the investigation. The variation of column spacing and the outer column diameter changed the water-plane area, the inertia moment, and the displacement volume, which affected the draft and stability of the floating foundation. Therefore, further research should be carried out in future to consider other structural parameters and the stability of the floating foundation, and to further the optimization of the FOWT.

**Author Contributions:** Conceptualization, Z.C.; methodology, Z.C.; software, S.L. and K.W.; validation, S.L. and X.L.; formal analysis, S.L.; investigation, S.L. and X.L.; resources, Z.C.; data curation, Z.C.; writing—original draft preparation, S.L.; writing—review and editing, Z.C., X.C., L.H. and K.W.; visualization, S.L. and Z.C.; supervision, Z.C.; project administration, X.C. and L.H.; funding acquisition, Z.C., X.C. and L.H. All authors have read and agreed to the published version of the manuscript.

**Funding:** This research was funded by National Key Research and Development Program (Grant No. 2022YFE0107000); National Natural Science Foundation of China (Grant No. 52171259); Dalian Science and Technology Innovation Fund Project (No. 2020JJ25CY016); Fundamental Research Funds for the Central University (3132022122); State Key Laboratory of Coastal and Offshore Engineering Fund (LP2115).

**Institutional Review Board Statement:** Not applicable.

**Informed Consent Statement:** Not applicable.

**Data Availability Statement:** All data in this study has been included in this paper.

**Conflicts of Interest:** The authors declare no conflict of interest.

## References

1. DNV. *Ocean's Future to 2050*; DNV: Dublin, OH, USA, 2021.
2. Lee, J.; Zhao, F. *GWEC Global Wind Report 2022*; Global Wind Energy Council: Brussels, Belgium, 2022.
3. Failla, G.; Arena, F. New perspectives in offshore wind energy. *Philos. Trans. R. Soc. A Math. Phys. Eng. Sci.* **2015**, *373*, 20140228. [[CrossRef](#)] [[PubMed](#)]
4. Chuang, Z.; Liu, S.; Lu, Y. Influence of second order wave excitation loads on coupled response of an offshore floating wind turbine. *Int. J. Nav. Archit. Ocean. Eng.* **2020**, *12*, 367–375. [[CrossRef](#)]
5. Zhao, Z.; Wang, W.; Shi, W.; Li, X. Effects of second-order hydrodynamics on an ultra-large semi-submersible floating offshore wind turbine. *Structures* **2020**, *28*, 2260–2275. [[CrossRef](#)]
6. Liu, S.; Chuang, Z.; Li, C. Dynamic Performance Evaluation of an Integrated 15 MW Floating Offshore Wind Turbine under Typhoon and ECD Condition. *Front. Energy Res.* **2022**, *10*, 354. [[CrossRef](#)]
7. Zhou, S. *Substructure Optimization of Semi-Submersible Floating Wind Turbines Based on Quick Dynamic Analysis*. Ph.D. Thesis, Harbin Institute of Technology, Harbin, China, 2021.
8. Ren, Y.; Venugopal, V.; Shi, W. Dynamic analysis of a multi-column TLP floating offshore wind turbine with tendon failure scenarios. *Ocean. Eng.* **2022**, *245*, 110472. [[CrossRef](#)]
9. Yi, Q. *Research on Dynamics Response and Structural Properties of Floating Wind Turbines Under Wind-Wave Condition in South China Sea*. Master's Thesis, Tsinghua University, Beijing, China, 2017.
10. Wei, D.; Que, X.; Fu, T.; Zhou, Y.; Du, J.; Wang, J. Research on Hydrodynamic Characteristics of a New Semi-submersible Floating Foundation for Offshore Wind Turbine. *Ocean. Eng.* **2022**, *40*, 82–92.
11. Li, J. *A New Floating Platform Design and the Coupled Dynamic Analysis of the Offshore Wind Turbine System*. Ph.D. Thesis, Tianjin University, Tianjin, China, 2014.
12. Wang, Y.; Shi, W.; Michailides, C.; Wan, L.; Kim, H.; Li, X. WEC shape effect on the motion response and power performance of a combined wind-wave energy converter. *Ocean. Eng.* **2022**, *250*, 111038. [[CrossRef](#)]
13. Cao, Q.; Xiao, L.; Guo, X.; Liu, M. Second-order responses of a conceptual semi-submersible 10 MW wind turbine using full quadratic transfer functions. *Renew. Eng.* **2020**, *153*, 653–668. [[CrossRef](#)]
14. Wei, X.; Zhao, X. Vibration suppression of a floating hydrostatic wind turbine model using bidirectional tuned liquid column mass damper. *Wind. Energy* **2020**, *23*, 1887–1904. [[CrossRef](#)]
15. Aboutalebi, P.; M'zoughi, F.; Martija, I.; Garrido, I.; Garrido, A.J. Switching control strategy for oscillating water columns based on response amplitude operators for floating offshore wind turbines stabilization. *Appl. Sci.* **2021**, *11*, 5249. [[CrossRef](#)]
16. Haji, M.N.; Kluger, J.M.; Sapsis, T.P.; Slocum, A.H. A symbiotic approach to the design of offshore wind turbines with other energy harvesting systems. *Ocean. Eng.* **2018**, *169*, 673–681. [[CrossRef](#)]
17. Allen, C.; Viscelli, A.; Dagher, H.; Goupee, A.; Gaertner, E.; Abbas, N.; Hall, M.; Barter, G. *Definition of the UMaine VoltornUS-S Reference Platform Developed for the IEA Wind 15-Megawatt Offshore Reference Wind Turbine*; National Renewable Energy Lab. (NREL): Golden, CO, USA, 2020.
18. Niranjana, R.; Ramisetti, S.B. Insights from detailed numerical investigation of 15 MW offshore semi-submersible wind turbine using aero-hydro-servo-elastic code. *Ocean. Eng.* **2022**, *251*, 111024. [[CrossRef](#)]
19. Wu, J.; Kim, M.-H. Generic Upscaling Methodology of a Floating Offshore Wind Turbine. *Energies* **2021**, *14*, 8490. [[CrossRef](#)]
20. SINTEF Ocean. *SIMA Theory Manual*; SINTEF Ocean: Trondheim, Norway, 2020.
21. Moriarty, P.J.; Hansen, A.C. *AeroDyn Theory Manual*; National Renewable Energy Lab.: Golden, CO, USA, 2005.
22. Faltinsen, O. *Sea Loads on Ships and Offshore Structures*; Cambridge University Press: Cambridge, UK, 1993; Volume 1.
23. Morison, J.; Johnson, J.; Schaaf, S. The force exerted by surface waves on piles. *J. Pet. Technol.* **1950**, *2*, 149–154. [[CrossRef](#)]
24. SINTEF Ocean. *SIMO Theory Manual*; SINTEF Ocean: Trondheim, Norway, 2020.
25. DNVGL. *HydroD User Manual*; DNV: Dublin, OH, USA, 2017.
26. Faltinsen, O.M. Prediction of resistance and propulsion of a ship in a seaway. In Proceedings of the 13th Symposium on Naval Hydrodynamics, Tokyo, Japan, 6–10 October 1980.
27. SINTEF Ocean. *RIFLEX Theory Manual*; SINTEF Ocean: Trondheim, Norway, 2020.
28. SINTEF Ocean. Sintef Ocean Website. Available online: <https://www.sintef.no/programvare/sima/> (accessed on 8 July 2022).

29. Gaertner, E. *Definition of the IEA Wind 15-Megawatt Offshore Reference Wind Turbine*; NREL/TP-5000-75698; Technical Report; National Renewable Energy Laboratory: Golden, CO, USA, 2020.
30. DNVGL. DNV GL-Digital Solutions Website. Available online: <https://www.dnv.com/software> (accessed on 8 July 2022).
31. DNVGL. *Wadam User Manual*; DNV: Dublin, OH, USA, 2017.
32. WAMIT, Inc. Wamit Website. Available online: <https://www.wamit.com/index.htm> (accessed on 8 July 2022).
33. Wen, Y.; Wang, W.; Liu, H.; Mao, L.; Mi, H.; Wang, W.; Zhang, G. A shape optimization method of a specified point absorber wave energy converter for the south china sea. *Energies* **2018**, *11*, 2645. [[CrossRef](#)]
34. DNVGL. Volume DNVGL-OS-E301. In *Position Mooring*; DNV: Dublin, OH, USA, 2020.